Analytica Chimica Acta 1278 (2023) 341760

Contents lists available at ScienceDirect

Analytica Chimica Acta

journal homepage: www.elsevier.com/locate/aca

Synergetic-effect-enhanced electrochemiluminescence of zein-protected Au–Ag bimetallic nanoclusters for CA15-3 detection

Qiuyu Huang [a], Xiaodi Zhu [a], Xiaojun Sun [a], Xueying Wang [a], Yuyang Li [a], Hongmin Ma [a,*], Huangxian Ju [a,b], Qin Wei [a,c,**]

[a] Collaborative Innovation Center for Green Chemical Manufacturing and Accurate Detection, Key Laboratory of Interfacial Reaction & Sensing Analysis in Universities of Shandong, School of Chemistry and Chemical Engineering, University of Jinan, Jinan, 250022, Shandong. China
[b] State Key Laboratory of Analytical Chemistry for Life Science, Department of Chemistry, Nanjing University, Nanjing, 210023, China
[c] Department of Chemistry, Sungkyunkwan University, Suwon, 16419, Republic of Korea

HIGHLIGHTS

- The first present of zein as a protective ligand in electrochemiluminescent system.
- Au–Ag synergistic effect enhanced electrochemiluminescence of the cluster.
- GO-PANI is a co-reactant catalyst which has large specific surface area.
- The sensor can detect CA15-3 sensitively and with a detection limit of 0.0003 U mL^{-1}.

GRAPHICAL ABSTRACT

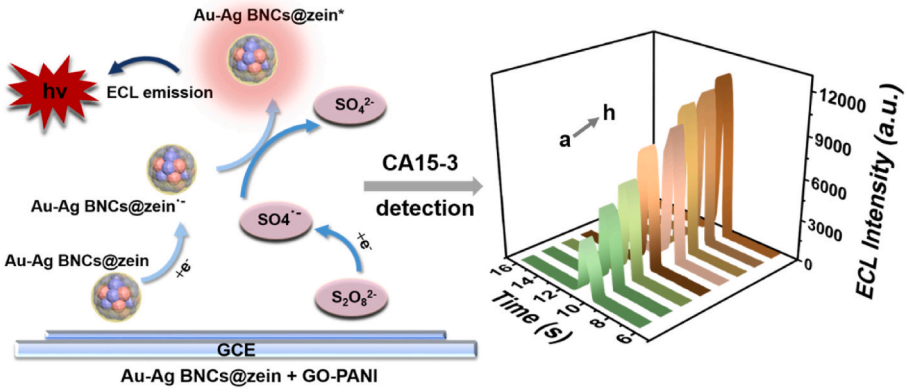

ARTICLE INFO

Handling Editor: Dr Jing-Juan Xu

Keywords:
Electrochemiluminescence biosensor
Zein
Gold-silver bimetallic nanoclusters
CA15-3

ABSTRACT

In this work, a sandwich-type electrochemiluminescence (ECL) system was constructed for the detection of CA15-3. Gold-silver bimetallic nanoclusters (Au–Ag BNCs) with zein as a protective ligand were synthesized, and the excellent ECL performance of this material was demonstrated for the first time. Zein carrying a variety of groups that ligated with Au–Ag BNCs, forming a protective shell of zein, effectively prevented clusters from aggregating or growing into larger nanoparticles. The synergistic effect of the bimetal promotes the ECL emission, making this nanoscale material an ideal ECL probe. GO-PANI, which effectively promoting the production of sulfate radicals of the co-reactant and significantly increasing the ECL strength, was a good sensing platform for antibody immobilization. Consequently, we constructed an ECL sensor with GO-PANI as the sensing platform

* Corresponding author.
** Corresponding author. Collaborative Innovation Center for Green Chemical Manufacturing and Accurate Detection, Key Laboratory of Interfacial Reaction & Sensing Analysis in Universities of Shandong, School of Chemistry and Chemical Engineering, University of Jinan, Jinan, 250022, Shandong. China.
E-mail addresses: chm_mahm@ujn.edu.cn (H. Ma), chm_weiq@ujn.edu.cn (Q. Wei).

https://doi.org/10.1016/j.aca.2023.341760
Received 9 August 2023; Received in revised form 27 August 2023; Accepted 28 August 2023
Available online 29 August 2023

and Au–Ag BNCs@zein as the ECL probe, with a detection range of 0.001–100 U mL^{-1} and a detection limit of 0.0003 U mL^{-1}, provided a strong support for the sensor for future CA15-3 detection applications.

1. Introduction

In today's world, where malignant tumors are a serious threat to the length and quality of people's lives, there is an immense and urgent need for early and sensitive diagnosis of cancer signature markers [1–3]. Breast cancer has the highest incidence rate among female cancers in the world, and glycoprotein 15-3 (CA15-3) is a specific immunomarker for breast cancer, and the level of CA15-3 changes significantly with the occurrence and changes of the disease, so the detection and monitoring of CA15-3 indexes provide important data for the early diagnosis of breast cancer, the evaluation of postoperative conditions and the observation of the efficacy of treatment [4–8]. Nowadays, various types of sensors have been developed for CA15-3 detection, such as photoelectrochemical sensors [9,10], fluorescent sensors [11,12], electrochemical sensors [13,14] and so on. The electrochemiluminescence sensor is based on the specific luminescence of the material on the surface of the electrode jumping from the excited state back to the ground state after high-energy electron transfer, which has the characteristics of lower background signal, higher sensitivity and better stability, and has also been widely used in the field of biomarker sensing [15–18].

In the field of ECL, common chemiluminescent reagents such as luminol have been widely used, so the exploration of new ECL luminophores is now a hot research topic [19,20], and metal nanoclusters have gradually come into the public eye because of their advantages of ultra-small size, high catalytic activity, and low toxicity [21–24]. For example, Ag NCs synthesized by song et al. [25] were used for the detection of calcitoninogen and Cu NCs synthesized by zhu et al. [26] were used for the detection of miRNA-21, both of which achieved lower detection limits and wider detection ranges. However, the low ECL emission signal and poor solution stability of single metal nanoclusters still need to be solved. The emergence of bimetallic nanoclusters [27] (BNCs) has solved the problem of the emission intensity of the ECL signal to a certain extent, and the synergistic effect of multiple atoms in itself makes it have extraordinary performance in electrochemistry and photochemistry, etc [28–31]. The stability problem can be solved by using proteins as a protective agent. The stability problem can be solved by using proteins as protective ligands, for example, zhai et al. [32] synthesized Au–Ag BNCs with bovine serum albumin (BSA) as a template, and applied them in the field of ECL sensing for the first time for the detection of Hg^{2+}, and the success of this sensor demonstrated that bimetallic nanoclusters involved in proteins combine the high emission of ECL signals with the high stability of clusters. of the ECL signal and high stability of the clusters.

However, most of the currently used proteins are animal proteins, which face the problems of high cost, unfriendly environment and complicated purification, so we introduced zein, a storage protein extracted from maize endosperm, into this system [33,34]. Zein has been widely used in electrostatic spinning and drug loading, which favorably demonstrated the good biocompatibility and environmental tolerance of zein; and another advantage of zein is its unique solubility, which can be easily and rapidly separated by diluting the solution or changing the pH of the solution, thus greatly saving the time and cost associated with traditional dialysis operations. Zein itself contains a

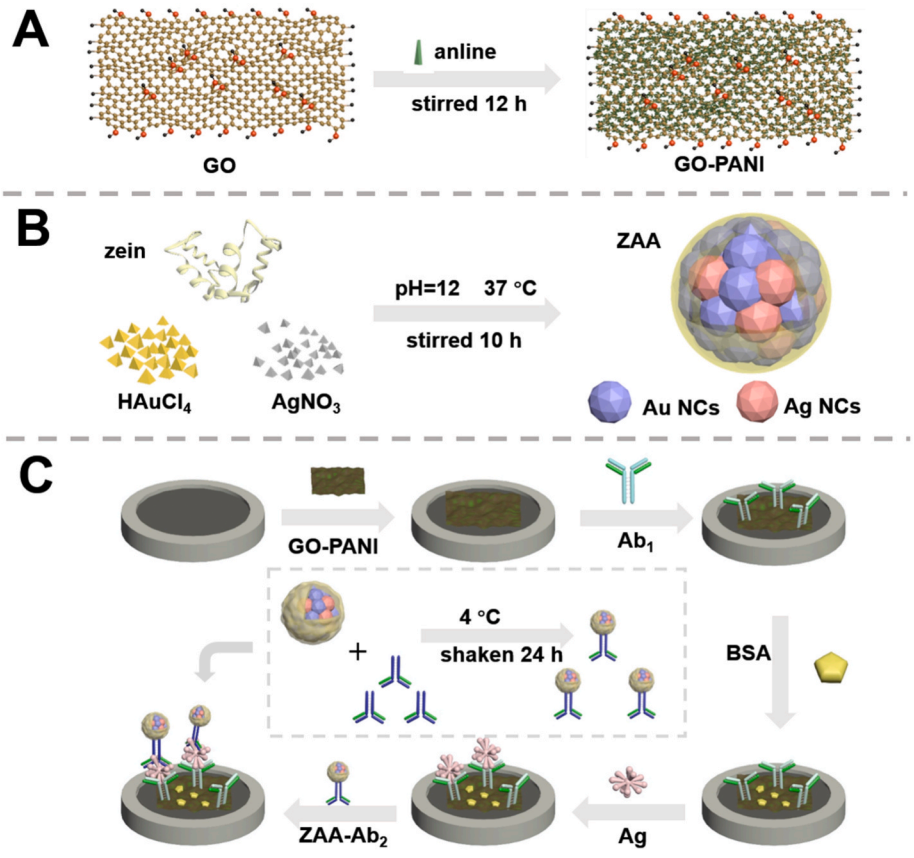

Scheme 1. (A): Synthesis process of GO-PANI. (B): Synthesis process of ZAA. (C): Fabrication process of CA15-3 biosensors.

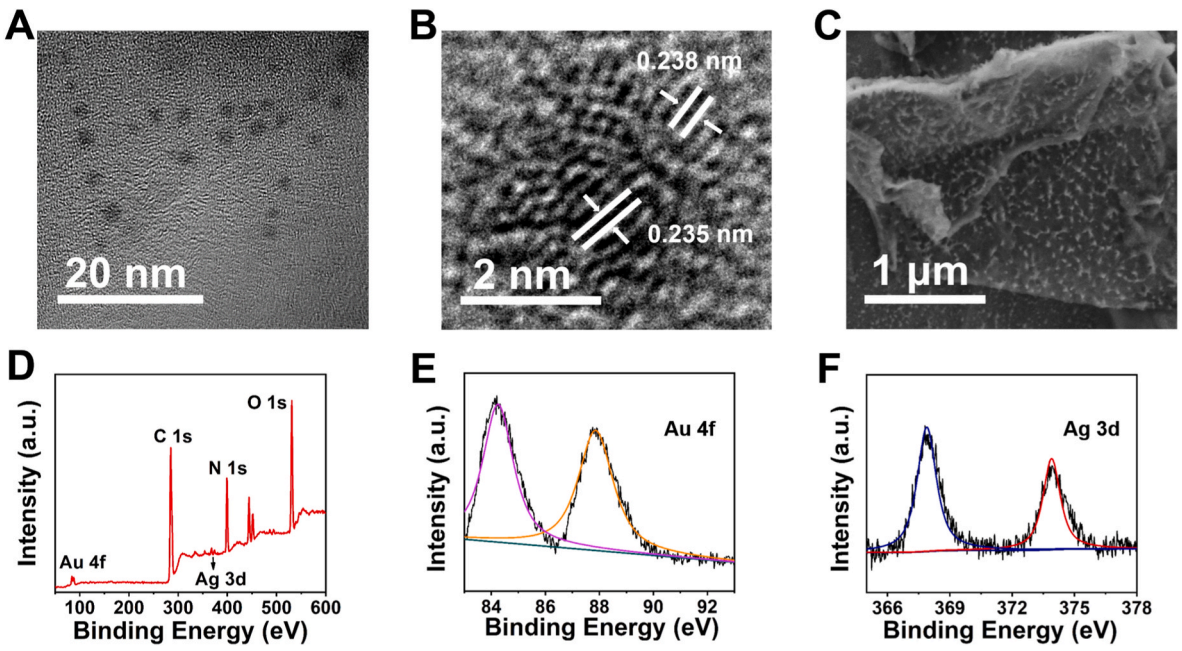

Fig. 1. (A): TEM and (B): HR-TEM images of ZAA. (C): SEM images of GO-PANI. (D): XPS full spectrum. (E): Au 4f region and (F): Ag 3d region of ZAA.

variety of amino acids, such as glutamine, leucine, and proline, which provide enough amino and carboxyl groups to coordinate with the metal [35–37]. Therefore, zein is the suitable choice of ligand for bimetallic nanocluster protection. However, zein has not been seen to have a wide range of applications in biosensing.

In this paper, we first carried out the reduction of Au–Ag BNCs (Au–Ag BNCs@zein) with zein as a protective ligand at alkaline low temperature and successfully isolated and purified them by adjusting the pH, and their protein outer layer also boosted the stable and high-intensity ECL emission from Au–Ag BNCs kept in solution for a long time. Therefore, we incubated Au–Ag BNCs@zein as a signaling tag with the secondary antibody (Ab_2). In order to further enhance the ECL signal intensity and better load the primary antibody (Ab_1), we chose graphene oxide with large specific surface area and multiple oxygen-containing functional groups and polyaniline composite (GO-PANI) with good catalytic activity as the substrate material for the sensor, which has numerous bioactive sites for immobilizing Ab_1 as well as good dispersion, and most importantly, it is good for this paper. The material has many bioactive sites to immobilize Ab_1 and good dispersion, and most importantly, it has excellent catalytic performance for the co-reactant $K_2S_2O_8$ used in this paper, and the emergence of more sulfate radicals will have more combinations with the Au–Ag BNCs, which will effectively improve the ECL emission intensity. Therefore, taking advantage of the above advantages, we constructed a sandwich-type immunosensor consisting of Au–Ag BNCs@zein as the Ab_2 marker and GO-PANI as the sensing platform for the detection of CA15-3. The detection range of this sensor was from 0.001 U mL^{-1} to 100 U mL^{-1}, and the detection limit was 0.0003 U mL^{-1} (S/N = 3), with good stability and detection performance. The good stability and detection performance of the sensor provides a strong support for the future application of CA15-3 detection.

2. Materials and methods

2.1. Preparation of GO-PANI

The synthesis of graphene oxide (GO) with oxygen-containing groups using the Hummers' method using graphite powder as a raw material [38]. The synthesis of GO-PANI is shown in Scheme 1 A. In the first step, 100 μL of aniline monomer was added to 40 mL of a solution containing 1 M H_2SO_4, which formed a white solid, and we chose to disperse it by sonication for 30 min to obtain a homogeneous solution. In the second step, we weighed 20 mg of GO solid and added 40 mL of ultrapure water for 4 h to obtain a well-dispersed GO solution at a concentration of 0.5 mg mL^{-1}, which was added to the aniline solution and stirred for 30 min. After stirring, 300 mg of $(NH_4)_2S_2O_8$ was slowly added to the solution for 12 h. The final color of the solution was dark green and the solution was washed by centrifugation at 9000 rpm until neutral and dried under vacuum at 60 °C. The resulting solid was a graphene oxide-polyaniline nanocomposite (GO-PANI).

2.2. Preparation of Au–Ag BNCs@zein

The synthesis of Au–Ag bimetallic nanoclusters (Au–Ag BNCs@zein) is shown in Scheme 1 B. 0.5 mL of 2 M NaOH solution was added to 4 mL of deionised water. 50 mg of zein powder was weighed and added to the above solution to dissolve, and the solution was clarified yellow. The solution was then prepared with 10 mM $AgNO_3$ and 2% $HAuCl_4{\cdot}3H_2O$, and 1.2 mL and 250 μL were added to the zein solution, respectively, to form a homogeneous solution under ultrasonication, and the mixture was adjusted to pH = 12 with NaOH and stirred at 37 °C for 10 h. After the reaction was completed, the precipitate was centrifuged at 5000 rpm for 5 min to obtain the precipitated material was removed and the supernatant was added to the solution with dilute sulphuric acid until a precipitate appeared. The solution was then centrifuged at 6000 rpm and the precipitate was dispersed in 3 mL of 2.5% $NH_3{\cdot}H_2O$ and incubated for 30 min at 80 °C. The final product was purified by centrifugation in isopropanol several times and the final product was dissolved in deionised water and volumetised to 1 mL, resulting in Au–Ag BNCs@zein (ZAA) stock solution. Zein-reduced simple Au NCs or Ag NCs was added to 10 mM $AgNO_3$ solution or 2% $HAuCl_4{\cdot}3H_2O$ solution by following the above procedure only.

2.3. Preparation of Au–Ag BNCs@zein-Ab_2

1 mL of 10 μg mL^{-1} of CA15-3 Ab_2 solution and 200 μL of ZAA stock solution were added to 5 mL of deionised water and incubated overnight at 4 °C. The resulting precipitate was washed by centrifugation to Au–Ag BNCs@zein-Ab_2 (ZAA-Ab_2) and dispersed in 1 mL of pH = 7.4 PBS to give a ZAA-labelled concentration of 1/5 and stored in a refrigerator at

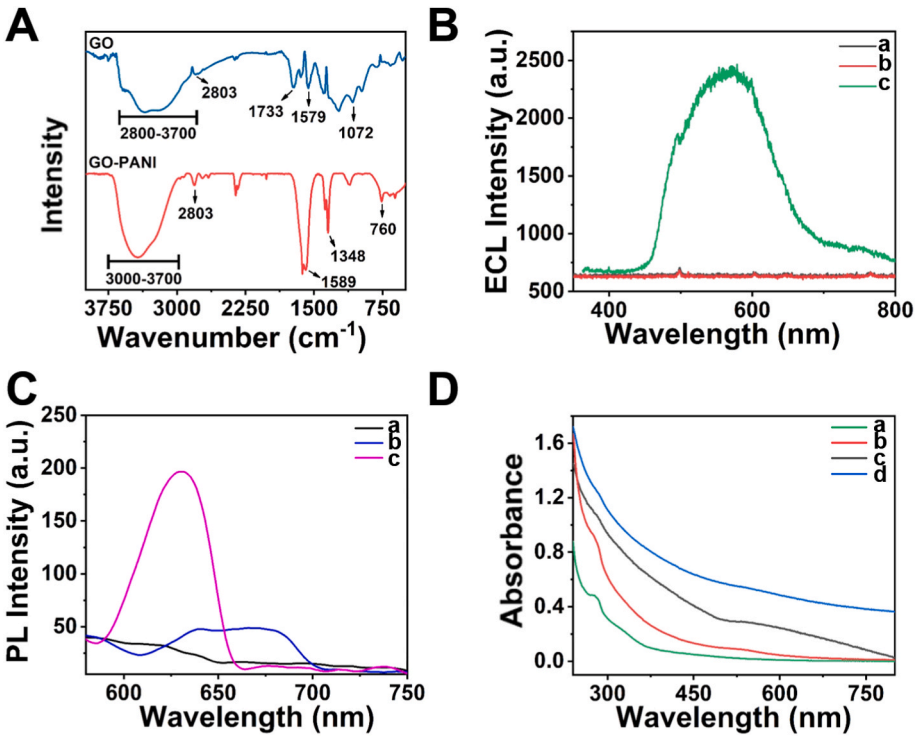

Fig. 2. (A): FT-IR spectra of GO (black line) and GO-PANI (red line). (B): ECL spectra of Au NCs@zein(a), Ag NCs@zein(b) and Au–Ag BNCs@zein(c). (C): FL spectra of Au NCs(a), Ag NCs(b) and Au–Ag BNCs@zein(c). (D): UV–vis absorption spectra of zein(a), Au–Ag BNCs@zein(b), Au NCs@zein(c), Ag NCs@zein(d). (For interpretation of the references to color in this figure legend, the reader is referred to the Web version of this article.)

4 °C until further use.

2.4. Construction of the ECL sensor

The sensor was constructed as shown in Scheme 1C. After polishing the electrode with alumina powder, 6 μL of GO-PANI solution at various concentrations was added dropwise, and the material catalyzed $K_2S_2O_8$ in the substrate to produce more $SO_4^{\bullet-}$ radicals and to load 6 μL of the primary antibody to CA15-3 (Ab_1) added dropwise in the next step. This was followed by the sequential addition of 3 μL of BSA solution (1%), various concentrations of CA15-3 antigen solution and 6 μL of ZAA-Ab_2 solution (labelled at 1/5th of the concentration). After each layer has been modified, the electrode should be dried at 4 °C and then washed with a pH = 7.4 PBS buffer solution to remove any unmodified material from the electrode. Finally, after the build is complete, the completed sensor is stored at 4 °C and awaits testing.

2.5. ECL testing

The correlation assay was performed using the ECL technique and the step-pulse method. ECL test was carried out in a pH = 8.0 PBS solution containing 100 mM $K_2S_2O_8$. The photomultiplier tube was operated at an operating voltage of 800 V, pulsed for 10 s at an initial potential of 0 V, and then pulsed for 1 s at a termination voltage of −1.6 V.

3. Results and discussion

3.1. Characterization of GO-PANI composites with Au–Ag BNCs@zein

In order to visualize the morphology and size of GO-PANI composites more intuitively, we carried out scanning electron microscopy tests. In Fig. 1 C, we can see that GO is in a lamellar and curled state, while PANI is uniformly distributed on the surface of GO and formed spicules. This figure demonstrates the large specific surface area of the GO lamellae and also the successful polymerisation of aniline on the GO lamellae. We also performed FT-IR spectrograms to confirm the successful synthesis of GO-PANI composites. As shown in Fig. 2 A, we see that there are two lines respectively. The blue line is attributed to GO and the red line is attributed to the GO-PANI composite. GO shows a broad absorption band between 2800 cm^{-1} and 3700 cm^{-1}, which we presume to be attributed to the absorption due to hydrogen bonding of OH. The peaks at 1733 cm^{-1} as well as 1579 cm^{-1} and 1072 cm^{-1}, we attribute to C═O, C–O in COOH and C–O in epoxy functional groups, respectively. Thus, we similarly demonstrate the successful synthesis of GO monomer. From the infrared spectra of GO-PANI composites we can see that the graph produces a broad absorption band between 3000 cm^{-1} and 3700 cm^{-1}, which originates from the infrared absorption of OH. The figure also produces three characteristic absorption bands at 1589 cm^{-1}, 1348 cm^{-1} and 760 cm^{-1}, which belong to C═N, C–N stretching vibration and C–H out-of-plane bending, respectively, and this result also indicates that COOH in GO produces a successful connection with N on the polyaniline skeleton.

For the synthesi zed Au–Ag BNCs@zein (ZAA), we carried out the characterization by high resolution transmission microscopy. From Fig. 1 A we can observe that the size of the clusters is between 2 and 3 nm, uniformly distributed and unaggregated. And from Fig. 1 B, two lattices are clearly demonstrated, and the lattice spacing is measured to be 0.238 nm and 0.235 nm, which are attributed to Ag (111) and Au (111) crystal surfaces, respectively. In order to further explore the elements contained on the surface of the synthesized materials and the valence states of the contained elements, we carried out XPS spectroscopy, as shown in Fig. 1 D, E and F. The peaks appearing at 84.1 eV and 87.9 eV for Au 4f then indicate the simultaneous presence of Au (0) and Au (I). And Au (I), which exists on the surface of the gold nuclei, can better maintain the stability of the clusters for the material's long-term stable preservation in aqueous medium. And the Ag 3d mode exhibits two strong peaks of Ag $3d_{5/2}$ (368 eV) and Ag $3d_{3/2}$ (374 eV), which are also well matched with the peaks of zero-valent Ag. The B plot of Fig. 2 shows the ECL spectra, and we can observe that the synthesized ZAA

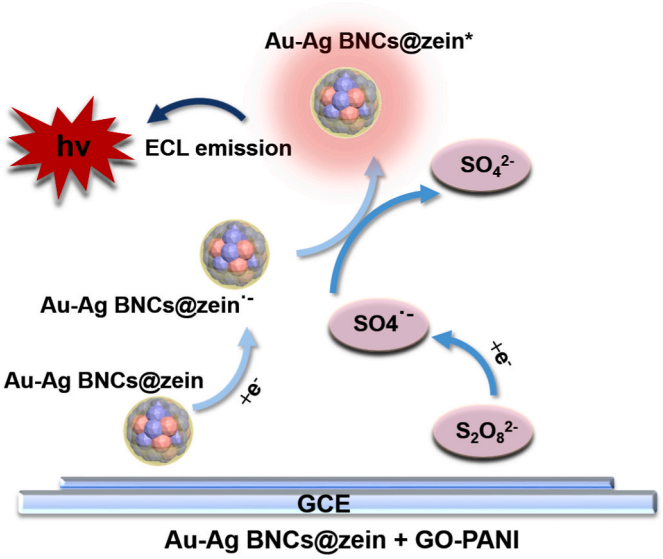

Scheme 2. Diagram of the possible ECL emission mechanism.

presents a superior ECL emission at 580 nm, whereas the other materials to which only $HAuCl_4$ or $AgNO_3$ were added during the synthesis process did not show their ECL emission properties, which we speculate is due to the change in the composition of the raw materials. The fluorescence spectra of ZAA are demonstrated in Fig. 2C. We can observe that Au NCSs do not show any significant fluorescence emission peaks, Ag NCs show a broader low peak between 610 and 700 nm, and Au–Ag BNCs show higher fluorescence emission at 630 nm, which confirms the successful synthesis of metal nanoclusters in synergistic manner with Au and Ag. The dispersion state of Au–Ag BNCs and its luminescence fluorescence photos under UV lamps in Fig. S1 The UV–vis spectra are shown in Fig. 2 D. The green line is attributed to zein, the red line is attributed to the synthesized material ZAA, and the black and blue lines are attributed to Au NCs and Ag NCs, respectively. The reason for the weaker peaks at the 255 nm of the last three curves is attributed to the process of synthesizing metal nanoclusters. The black line shows a broader absorption peak at 520 nm, which we attribute to the surface plasmon resonance of gold nanoparticles. In contrast, the blue curve with the addition of $AgNO_3$ only did not show a more pronounced characteristic absorption peak after 300 nm, and we hypothesized that this was because the measured solution was only the residual zein after synthesis, and the large silver nanoparticles that were originally formed were removed during centrifugation in the first step of the synthesis step. It also supports the fact that Au NCs and Ag NCs were not successfully synthesized under this synthesis condition. When we analyze the ZAA curve, we can see the characteristic peak of zein at 255 nm. The characteristic peak does not appear after 400 nm in the curve, and the characteristic peak of surface plasmon resonance does not appear clearly. Zein and ZAA have the same characteristic absorption peaks in FT-IR in Fig. S2, this also confirms the successful synthesis of the bimetallic nanocluster.

3.2. Possible ECL mechanism

We explored the ECL luminescence mechanism of ZAA as shown in Scheme 2. For the ECL test, we chose the step-pulse method as the electrochemical method for the test, specifying an initial potential of 0 V with a duration of 10 s and a termination potential of −1.6 V with a duration of 1 s. After the scanning, we obtained the superior ECL emission peaks presented by our synthesized material.

We speculate that the mechanism is that the ZAA material on the surface of the glassy carbon electrode gets electrons to generate $ZAA^{\bullet-}$ (Equation (1)), while at the same time, $S_2O_8^{2-}$ in the solution also gets electrons to generate $SO_4^{\bullet-}$ (Equation (2)), which possesses strong oxidizing property. When the reduced state of $ZAA^{\bullet-}$meets the strong oxidizing $SO_4^{\bullet-}$, the electrons of the two are transferred to each other at a potential of −1.6 V, resulting in ZAA* (Equation (3)), which is produced when the substance leaps from the excited state back to the ground state. Photons (Equation (4)), the ECL signal is then generated.

$$ZAA + e^- \rightarrow ZAA^{\bullet-} \quad (1)$$

$$S_2O_8^{2-} + e^- \rightarrow SO_4^{2-} + SO_4^{\bullet-} \quad (2)$$

$$ZAA^{\bullet-} + SO_4^{\bullet-} \rightarrow ZAA^* + SO_4^{2-} \quad (3)$$

$$ZAA^* \rightarrow ZAA + h\nu \quad (4)$$

In Fig. 3 A, we performed ECL tests on GCE (a), GCE/GO-PANI (b), GCE/ZAA (c), and GCE/GO-PANI/ZAA (d) in PBS buffer solution at pH = 8.0 and containing 100 mM $K_2S_2O_8$. As shown in the figure, GCE and GCE/GO-PANI presented lower ECL emission on the electrode surface, and the signal generation may be caused by the presence of a small amount of dissolved oxygen in the electrolyte, while in comparison we can find that the signal intensity of the luminescent body ZAA was enhanced by several times with GO-PANI as the electrode substrate material, so we speculate that GO-PANI may have a co-reactant catalyst.

In order to further investigate the effect of GO-PANI on $K_2S_2O_8$ we performed another CV scan of the material, as shown in Fig. 3 B, the bare electrode showed an obvious reduction peak at −1.15 V, while the reduction peak of GO-PANI appeared around 0.89 v. The comparison found that the latter out of the peak potential shifted positively obviously, which proved that the reduction process of $S_2O_8^{2-}$ was promoted, and the lowering of the reaction potential barriers also implied that the reduction of $S_2O_8^{2-}$ can occur at a lower potential (absolute value). We also performed electron paramagnetic resonance spectroscopy (EPR) tests on the GO-PANI composites, it confirms the existence of $SO_4^{\bullet-}$.

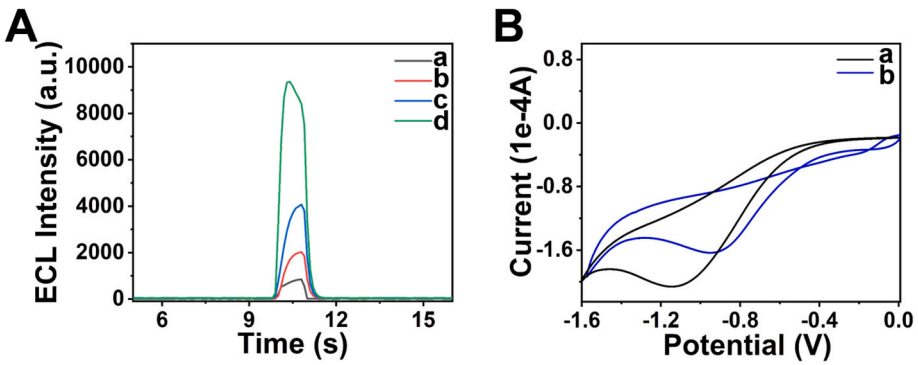

Fig. 3. (A): ECL emission of GCE(a), GCE/GO-PANI(b), GCE/ZAA(c) and GCE/GO-PANI/ZAA (d) in 100 mM $K_2S_2O_8$. (B): CV for produced electrodes in PBS including 100 mM $K_2S_2O_8$ of GCE(a) and GO-PANI(b).

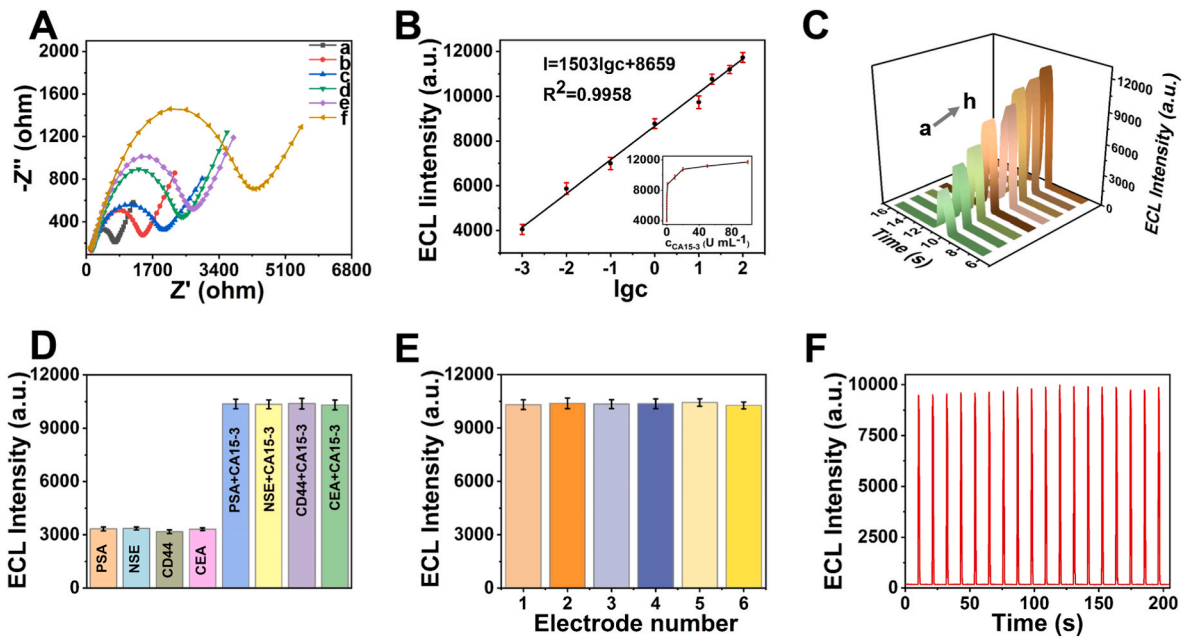

Fig. 4. (A): EIS impedance of the CA15-3 sensor layer modification process: GCE(a), GCE/GO-PANI(b), GCE/GO-PANI/Ab_1(c), GCE/GO-PANI/Ab_1/BSA(d), GCE/GO-PANI/Ab_1/BSA/Ag(e), GCE/GO-PANI/Ab_1/BSA/Ag/ZAA@Ab_2(f). (B): operating curve view, (C): 3D operating curve view, (D)selectivity, (E)reproducibility and (F)stability of the constructed biosensor.

From the above description of Fig. 3 A, B and Fig. S4, we can further confirm the existence of more $SO_4^{\bullet-}$ in the system which can collide and combine with our luminescent materials to produce strong and high ECL signals, and also validate our proposed signal amplification mechanism, the substrate material GO-PANI composite has a catalytic effect on the co-reactant $K_2S_2O_8$.

3.3. Sensor construction process

In order to verify the success of the constructed sensor with layer-by-layer modification, we tested its electrochemical impedance (EIS) map, which was carried out in $[Fe(CN)_6]^{3-/4-}$ solution. In Fig. 4 A, we can see that the impedance of the electrode surface is larger than that of the bare electrode surface when the GO-PANI composite is modified on the electrode surface, which is presumed to be triggered by the increase of the resistance due to the oxygen-containing functional groups in the graphene oxide in the substrate material. The subsequent radius also shows a gradual increasing trend, which is due to the fact that the bioactive substances added dropwise in each step are protein in nature, which also plays a hindering role in the transfer of electrons. Therefore, the EIS successfully proved the success of the electrode layer modification, and later we also carried out other characterization of the material during the construction process, which are the cyclic voltammogram (CV) graphs in Fig. S5 A and the ECL signal intensity graphs in Fig. S5 B, respectively. Both figures similarly confirm the success of the layer modification of the sensor.

3.4. Detection of CA15-3 by ECL sensor

Under the optimized experimental conditions (shown in Fig. S3) described above, we performed a series of working curve assays for CA15-3 antigen concentration as shown in Fig. 4 B and C. As the CA15-3 antigen concentration increased from 0.001 U mL^{-1} to 100 U mL^{-1}, the ECL signal emission we obtained showed a linear increase. After a linear fit to the data, we obtained the correction curve: I = 1503lgc+8659, where I is the ECL signal intensity lgc is the logarithm of the CA15-3 antigen concentration. The correlation coefficient was 0.9958 and the detection limit was 0.0003 U mL^{-1}. We compared this data with the sensor data collected for CA15-3 in the previous period, as shown in Table 1. The lower detection limit of our sensor as well as the wider detection range thus proved that our sensor has a good performance and is suitable for the series of CA15-3 antigen detection.

Table 1
Comparison of detection ranges and detection limits for each type of sensor.

Detection Method	Detection Range (U mL^{-1})	Detection Limit (U mL^{-1})	Reference
Electrochemical sensors	0.5–200	0.17	[39]
Chemiluminescent sensors	0–250	0.035	[40]
LSPR sensors	0–40	0.87	[41]
ECL sensors	0.005–500	0.0017	[42]
ECL sensors	0.001–100	0.0003	this article

The excellent performance of this sensor is also demonstrated in the good selectivity, reproducibility and stability, as shown in Fig. 4 D. When we replaced the detection antigens with PSA, NSE, CD44 and CEA, we obtained the ECL emission values nearly equal to the blank values; and when we chose to mix CA15-3 with other interfering substances (CA15-3 concentration of 1 U mL^{-1}) for the testing, the ECL signals obtained were almost the same as those of the same concentration in the working curve, which proved the good selectivity of the sensor. For the reproducibility test, the same antigen with a concentration of 1 U mL^{-1} was selected, and as shown in Fig. 4 E, the ECL signals obtained from the

Table 2
Sample detection and spiked recovery of ECL sensors.

Samples (U mL^{-1})	Addition (U mL^{-1})	Average (U mL^{-1}, n = 5)	RSD (%, n = 5)	Recovery %
2.51	1.00	3.49	2.6	98.0
	3.00	5.50	2.2	99.7
	5.00	7.69	1.3	104
4.69	2.00	6.72	1.7	102
	5.00	9.82	2.9	103
	7.00	11.6	1.8	98.7

six probes were almost the same, which verified the good reproducibility of the sensor. The stability of the sensor is demonstrated in Fig. 4 F. The antigen with a concentration of 1 U mL^{-1} was selected for a long time test of 200 s. An RSD = 2.6% was obtained, which verifies the good stability of the sensor.

3.5. Actual sample detection

In order to verify whether the prepared sensor can perform well in practical applications, we used the spiked recovery method to detect serum containing different concentrations of antigen, as shown in Table 2, the spiked recoveries of CA15-3 were in the range of 98.3%–103%, which indicates that the sensor prepared in this paper has a good prospect for the practical application of CEA.

4. Conclusion

In summary, we synthesized ZAA, a bimetallic nanocluster with gold and silver synergism, using zein as a protective ligand, and combined it with an antibody as a signal tag, then we synthesized GO-PANI, a co-reactive catalyst with multiple biologically active sites, as a sensing platform, and constructed an ultrasensitive sandwich-type electrochemiluminescence immunosensor for the detection of CA15-3. We obtained a low detection limit of 0.0003 U mL^{-1} and a wide detection range of 0.001 U mL^{-1} and 100 U mL^{-1}. The sensor showed excellent selectivity, reproducibility and stability, and the results of the samples confirmed the precision and accuracy of the sensor, which will provide more possibilities for the detection of CA15-3 in the future.

CRediT authorship contribution statement

Qiuyu Huang: Investigation, Conceptualization, Methodology, Writing – original draft. **Xiaodi Zhu:** Data curation. **Xiaojun Sun:** Software. **Xueying Wang:** Project administration, Funding acquisition. **Yuyang Li:** Writing – review. **Hongmin Ma:** Writing – review & editing, Project administration, Funding acquisition. **Huangxian Ju:** Resources. **Qin Wei:** Resources.

Declaration of competing interest

The authors declare that they have no known competing financial interests or personal relationships that could have appeared to influence the work reported in this paper.

Data availability

No data was used for the research described in the article.

Acknowledgments

This work was financially supported by the National Natural Science Foundation of China (22374059), the Shandong Provincial Natural Science Foundation (ZR2020YQ13), a Project of Shandong Province Higher Educational Youth Innovation Science and Technology Program (2020KJC008), and the Young Taishan Scholars Program of Shandong Province of China.

Appendix A. Supplementary data

Supplementary data to this article can be found online at https://doi.org/10.1016/j.aca.2023.341760.

References

[1] F. Bray, J. Ferlay, I. Soerjomataram, R.L. Siegel, L.A. Torre, A. Jemal, Global cancer statistics 2018: GLOBOCAN estimates of incidence and mortality worldwide for 36 cancers in 185 countries, Ca-Cancer J. Clin. 68 (2018) 394–424.
[2] X.J. Liu, Y.C. Zhao, F. Li, Nucleic acid-functionalized metal-organic framework for ultrasensitive immobilization-free photoelectrochemical biosensing, Biosens. Bioelectron. 173 (2021) 7.
[3] S.C. Song, N. Li, L.P. Bai, P.P. Gai, F. Li, Photo-Assisted robust anti-interference self-powered biosensing of MicroRNA based on Pt-S bonds and the inorganic-organic hybridization strategy, Anal. Chem. 94 (2022) 1654–1660.
[4] S. Akbari Nakhjavani, B. Khalilzadeh, P. Samadi Pakchin, R. Saber, M. H. Ghahremani, Y. Omidi, A highly sensitive and reliable detection of CA15-3 in patient plasma with electrochemical biosensor labeled with magnetic beads, Biosens. Bioelectron. 122 (2018) 8–15.
[5] X.-Y. Ge, Y.-G. Feng, S.-Y. Cen, A.-J. Wang, L.-P. Mei, X. Luo, J.-J. Feng, A label-free electrochemical immnunosensor based on signal magnification of oxygen reduction reaction catalyzed by uniform PtCo nanodendrites for highly sensitive detection of carbohydrate antigen 15-3, Anal. Chim. Acta 1176 (2021), 338750.
[6] M. Hasanzadeh, S. Tagi, E. Solhi, N. Shadjou, A. Jouyban, A. Mokhtarzadeh, Immunosensing of breast cancer prognostic marker in adenocarcinoma cell lysates and unprocessed human plasma samples using gold nanostructure coated on organic substrate, Int. J. Biol. Macromol. 118 (2018) 1082–1089.
[7] S. Jeong, M.-J. Park, W. Song, H.-S. Kim, Current immunoassay methods and their applications to clinically used biomarkers of breast cancer, Clin. Biochem. 78 (2020) 43–57.
[8] A.-J. Wang, X.-Y. Zhu, Y. Chen, X. Luo, Y. Xue, J.-J. Feng, Ultrasensitive label-free electrochemical immunoassay of carbohydrate antigen 15-3 using dendritic Au@Pt nanocrystals/ferrocene-grafted-chitosan for efficient signal amplification, Sensor. Actuator. B Chem. 292 (2019) 164–170.
[9] J.L.B. Neto, T.S. Martins, S.A.S. Machado, O.N. Oliveira, Enhanced photocatalysis on graphitic carbon nitride sensitized with gold nanoparticles for photoelectrochemical immunosensors, Appl. Surf. Sci. 606 (2022), 154952.
[10] M.X. Peng, S.Y. Lin, Z.B. Lin, D.L. Zheng, Y.B. Song, F.S. Lu, Y.W. Chen, W.H. Gao, Rationally constructed ZnCdS-HDCs@In_2S_3-HNRs double-hollow heterojunction with promoted light capture capability for photoelectrochemical biosensing, Biosens. Bioelectron. 201 (2022), 113957.
[11] N. Li, Y. Jiang, T.Y. Lv, G.Y. Li, F. Yang, Immunofluorescence analysis of breast cancer biomarkers using antibody-conjugated microbeads embedded in a microfluidic-based liquid biopsy chip, Biosens. Bioelectron. 216 (2022), 114598.
[12] Y.W. Wu, X.L. Chen, X.F. Wang, M. Yang, F.L. Xu, C.J. Hou, D.Q. Huo, A fluorescent biosensor based on prismatic hollow Metal-polydopamine frameworks and 6-carboxyfluorescein (FAM)-labeled protein aptamer for CA15-3 detection, Sensor. Actuator. B Chem. 329 (2021), 129249.
[13] J. Amani, A. Khoshroo, M. Rahimi-Nasrabadi, Electrochemical immunosensor for the breast cancer marker CA 15-3 based on the catalytic activity of a CuS/reduced graphene oxide nanocomposite towards the electrooxidation of catechol, Microchim. Acta 185 (2018) 79.
[14] V.P. Gajdosova, L. Lorencova, P. Kasak, M. Jerigova, D. Velic, L. Orovcik, M. Barath, P. Farkas, J. Tkac, Redox features of hexaammineruthenium(III) on MXene modified interface: three options for affinity biosensing, Anal. Chim. Acta 1227 (2022), 340310.
[15] Z. Liu, W. Qi, G. Xu, Recent advances in electrochemiluminescence, Chem. Soc. Rev. 44 (2015) 3117–3142.
[16] H.L. Qi, C.X. Zhang, Z. Huang, L. Wang, W.N. Wang, A.J. Bard, Electrochemistry and electrogenerated chemiluminescence of 1,3,5-Tri(anthracen-10-yl)-benzene-Centered starburst oligofluorenes, J. Am. Chem. Soc. 138 (2016) 1947–1954.
[17] L. Zhao, X.Z. Song, X. Ren, D.W. Fan, Q. Wei, D. Wu, Rare self-luminous mixed-valence Eu-mof with a self-enhanced characteristic as a near-infrared fluorescent ECL probe for nondestructive immunodetection, Anal. Chem. 93 (2021) 8613–8621.
[18] W.X. Lv, Q.T. Yang, Q. Li, H.Y. Li, F. Li, Quaternary ammonium salt-functionalized tetraphenylethene derivative boosts electrochemiluminescence for highly sensitive aqueous-phase biosensing, Anal. Chem. 92 (2020) 11747–11754.
[19] Y. An, Y. Ren, M. Bick, A. Dudek, E.H.W. Waworuntu, J. Tang, J. Chen, B.S. Chang, Highly fluorescent copper nanoclusters for sensing and bioimaging (vol 154, 112078, 2020), Biosens. Bioelectron. 156 (2020), 112127.
[20] S.H. Chen, Z.Z. Huang, Q. Jia, Electrostatically confined in -situ preparation of stable glutathione-capped copper nanoclusters for fluorescence detection of lysozyme, Sensor. Actuator. B Chem. 319 (2020), 128305.
[21] Y. Jin, C. Zhang, X.Y. Dong, S.Q. Zang, T.C.W. Mak, Shell engineering to achieve modification and assembly of atomically-precise silver clusters, Chem. Soc. Rev. 50 (2021) 2297–2319.
[22] K.Y. Zheng, J.P. Xie, Engineering ultrasmall metal nanoclusters as promising theranostic agents, Trends Chem 2 (2020) 665–679.
[23] Y. Zhou, Y.Q. Yu, Y.Q. Chai, R. Yuan, Electrochemical synthesis of silver nanoclusters on electrochemiluminescent resonance energy transfer amplification platform for Apo-A1 detection, Talanta 181 (2018) 32–37.
[24] Q. Li, J.H. Wu, Q.T. Yang, H.Y. Li, F. Li, pH and redox dual-response disulfide bond-functionalized red-emitting gold nanoclusters for monitoring the contamination of organophosphorus pesticides in foods, Anal. Chem. 93 (2021) 7362–7368.
[25] X.Z. Song, L. Zhao, N. Zhang, L. Liu, X. Ren, H.M. Ma, X. Kuang, Y.Y. Li, C.N. Luo, Q. Wei, Ultrasensitive electrochemiluminescence biosensor with silver nanoclusters as a novel signal probe and alpha-Fe_2O_3-Pt as an efficient Co-reaction accelerator for procalcitonin immunoassay, Anal. Chem. 95 (2023) 1582–1588.

[26] X. Zhu, L.L. Liu, W.W. Cao, R. Yuan, H.J. Wang, Ultra-sensitive MicroRNA biosensor based on strong aggregation-induced electrochemiluminescence from bidentate ligand-stabilized copper nanoclusters in polymer hydrogel, Anal. Chem. 95 (2023) 5553–5560.
[27] S.L. Christensen, M.A. MacDonald, A. Chatt, P. Zhang, H.F. Qian, R.C. Jin, Dopant location, local structure, and electronic properties of Au24Pt(SR)(18) nanoclusters, J. Phys. Chem. C 116 (2012) 26932–26937.
[28] S.X. Wang, Y.B. Song, S. Jin, X. Liu, J. Zhang, Y. Pei, X.M. Meng, M. Chen, P. Li, M. Z. Zhu, Metal exchange method using Au-25 nanoclusters as templates for alloy nanoclusters with atomic precision, J. Am. Chem. Soc. 137 (2015) 4018–4021.
[29] H.J. Zhang, T. Watanabe, M. Okumura, M. Haruta, N. Toshima, Catalytically highly active top gold atom on palladium nanocluster, Nat. Mater. 11 (2012) 49–52.
[30] B. Zugic, L.C. Wang, C. Heine, D.N. Zakharov, B.A.J. Lechner, E.A. Stach, J. Biener, M. Salmeron, R.J. Madix, C.M. Friend, Dynamic restructuring drives catalytic activity on nanoporous gold-silver alloy catalysts, Nat. Mater. 16 (2017) 558–564.
[31] B.Z. Zheng, J.Y. Zheng, T.T. Yu, A.H. Sang, J. Du, Y. Guo, D. Xiao, M.M.F. Choi, Fast microwave-assisted synthesis of AuAg bimetallic nanoclusters with strong yellow emission and their response to mercury(II) ions, Sensor. Actuator. B Chem. 221 (2015) 386–392.
[32] Q.F. Zhai, H.H. Xing, X.W. Zhang, J. Li, E. Wang, Enhanced electrochemiluminescence behavior of gold-silver bimetallic nanoclusters and its sensing application for mercury(II), Anal. Chem. 89 (2017) 7788–7794.
[33] S. Babitha, P.S. Korrapati, TiO_2 immobilized zein microspheres: a biocompatible adsorbent for effective dye decolourisation, RSC Adv. 5 (2015) 26475–26481.
[34] E. Blanco-Garcia, F.J. Otero-Espinar, J. Blanco-Mendez, J.M. Leiro-Vidal, A. Luzardo-Alvarez, Development and characterization of anti-inflammatory activity of curcumin-loaded biodegradable microspheres with potential use in intestinal inflammatory disorders, Int. J. Pharm. 518 (2017) 86–104.
[35] H. Li, Y.K. Yuan, J.X. Zhu, T. Wang, D.F. Wang, Y. Xu, Zein/soluble soybean polysaccharide composite nanoparticles for encapsulation and oral delivery of lutein, Food Hydrocolloids 103 (2020), 105715.
[36] L. Mahalakshmi, M.M. Leena, J.A. Moses, C. Anandharamakrishnan, Micro- and nano-encapsulation of beta-carotene in zein protein: size-dependent release and absorption behavior, Food Funct. 11 (2020) 1647–1660.
[37] J.J.L. Wong, A.I.C. Wong, Y.Y. Xu, O. Yuliarti, Zein as a water insoluble excipient for spray dry encapsulation of hydrophilic bioactives, J. Food Eng. 283 (2020), 110054.
[38] W.S. Hummers Jr., R.E. Offeman, Preparation of graphitic oxide, J. Am. Chem. Soc. 80 (1958) 1339, 1339.
[39] A.J. Wang, X.Y. Zhu, Y. Chen, X.L. Luo, Y.D. Xue, J.J. Feng, Ultrasensitive label-free electrochemical immunoassay of carbohydrate antigen 15-3 using dendritic Au@Pt nanocrystals/ferrocene-grafted-chitosan for efficient signal amplification, Sensor. Actuator. B Chem. 292 (2019) 164–170.
[40] Y.-M. Liu, Y.-L. Zheng, J.-T. Cao, Y.-H. Chen, F.-R. Li, Sensitive detection of tumor marker CA15-3 in human serum by capillary electrophoretic immunoassay with chemiluminescence detection, J. Separ. Sci. 31 (2008) 1151–1155.
[41] Z.Y. Fan, Z.X. Geng, W.H. Fang, X.Q. Lv, Y. Su, S.C. Wang, H.D. Chen, Smartphone biosensor system with multi-testing unit based on localized surface plasmon resonance integrated with microfluidics chip, Sensors 20 (2020) 446.
[42] D.M. Qin, X.H. Jiang, G.C. Mo, J.S. Feng, C.H. Yu, B.Y. Deng, A novel carbon quantum dots signal amplification strategy coupled with sandwich electrochemiluminescence immunosensor for the detection of CA15-3 in human serum, ACS Sens. 4 (2019) 504–512.